

ALMA observations of super-early galaxies: Attenuation-free model predictions

A. Ferrara^{1,*}, S. Carniani¹, F. di Mascia¹, R. J. Bouwens², P. Oesch^{3,4}, and S. Schouws²

¹ Scuola Normale Superiore, Piazza dei Cavalieri 7, 56126 Pisa, Italy

² Leiden Observatory, Leiden University, NL-2300 RA Leiden, Netherlands

³ Observatoire de Genève, 1290 Versoix, Switzerland

⁴ Cosmic Dawn Center (DAWN), Niels Bohr Institute, University of Copenhagen, Jagtvej 128, København N DK-2200, Denmark

Received 25 September 2024 / Accepted 14 January 2025

ABSTRACT

The abundance and blue color of the super-early (redshift $z > 10$) luminous galaxies discovered by the *James Webb* Space Telescope (JWST) can be explained if radiation-driven outflows have ejected their dust on kiloparsec-scales. To test this hypothesis, we predict the Atacama Large Millimeter Array (ALMA) detectability of this extended dust component. Based on the observed properties of the galaxy, its observed continuum flux at 88 μm , F_{88} , depends on the dust-to-stellar mass ratio, ξ_d , and on the extent of the dust distribution, r_d . When this is applied to the most distant known galaxy, GS-z14-0 at $z = 14.32$, the fiducial model ($\xi_d = 1/529$) predicts $F_{88}^{\text{fid}} = 14.9 \mu\text{Jy}$ and a dust extent $r_d = 1.4 \text{ kpc}$. If the galaxy is very dust rich ($\xi_d = 1/40$), $F_{88}^{\text{max}} = 40.1 \mu\text{Jy}$. These values are lower ($F_{88}^{\text{fid}} = 9.5 \mu\text{Jy}$) if the dust is predominantly made of large grains such as those that form in supernova ejecta. Forthcoming ALMA observations might come very close to constraining the fiducial predictions of the outflow-based attenuation-free model. Other super-early galaxies are predicted to be fainter at 88 μm , mostly because their star formation rate is lower than that of GS-z14-0, with fiducial fluxes in the range 2–5.2 μJy .

Key words. galaxies: high-redshift

1. Introduction

The approximately 15 galaxies that have been discovered so far by the *James Webb* Space Telescope (JWST) at redshift $z > 10$ (Naidu et al. 2022; Arrabal Haro et al. 2023a; Hsiao et al. 2024; Wang et al. 2023; Fujimoto et al. 2023a; Atek et al. 2023; Curtis-Lake et al. 2023; Bunker et al. 2023; Tacchella et al. 2023; Arrabal Haro et al. 2023b; Finkelstein et al. 2023; Castellano et al. 2024; Zavala et al. 2025; Helton et al. 2024; Carniani et al. 2024a; Robertson et al. 2024) have raised a number of questions concerning early galaxy evolution. Not only does their number significantly overshoot extrapolations and models anchored at lower redshifts, these objects also share some peculiar properties whose origin constitutes a challenging puzzle for ΛCDM -based¹ galaxy formation scenarios.

At odds with their lower-redshift counterparts, many super-early galaxies are characterized by bright UV luminosities ($M_{\text{UV}} \lesssim -20$), and steep UV spectral slopes ($\beta \lesssim -2.2$), compact sizes (effective radius $r_e \approx 200 \text{ pc}$). The analysis of their spectral energy distribution suggests high (for their epoch) stellar masses ($M_\star \approx 10^9 M_\odot$), and thus identifies these rare systems as high- σ peaks of the cosmic density field that populate the bright end

of the luminosity function. Several alternative hypotheses have been suggested to explain the above properties².

According to the so-called attenuation-free model (AFM; Ferrara et al. 2023; Ziparo et al. 2023; Fiore et al. 2023; Ferrara 2024a,b), bright luminosities and blue colors result from extremely low dust attenuation conditions. These might be due to a low absorbing dust column density or to grain optical properties that produce gray relatively transparent extinction curves (see, e.g. Markov et al. 2024) at high redshift.

The AFM postulates that dust has been produced in supernova (SN) ejecta with a standard net³ yield $y_d \approx 0.1 M_\odot/\text{SN}$. Although it was corroborated by theoretical and observational work (Nozawa et al. 2010), this yield remains uncertain and even more so in the early Universe. Therefore, we allowed the dust-to-stellar mass ratio to vary by >3 orders of magnitude (see Sect. 2). After their injection into the interstellar medium, grains could either grow by gas-phase heavy element accretion and/or be partially destroyed by shocks. However, at $z > 10$ the prevailing physical conditions result in timescales of both processes that are longer than the Hubble time. This means that they are ineffective (Ferrara et al. 2016; Hirashita & Aoyama 2019; Martínez-González et al. 2019; Leśniewska & Michałowski

* Corresponding author; andrea.ferrara@sns.it

¹ Throughout the paper, we assume a flat Universe with the following cosmological parameters: $\Omega_M = 0.3075$, $\Omega_\Lambda = 1 - \Omega_M$, and $\Omega_b = 0.0486$, $h = 0.6774$, $\sigma_8 = 0.826$, where Ω_M , Ω_Λ , and Ω_b are the total matter, vacuum, and baryon densities in units of the critical density; h is the Hubble constant in units of 100 km s^{-1} , and σ_8 is the late-time fluctuation amplitude parameter (Planck Collaboration XVI 2014).

² These include (a) star formation variability (Mason et al. 2023; Mirocha & Furlanetto 2023; Pallottini & Ferrara 2023), (b) reduced feedback resulting in a higher star formation efficiency (Dekel et al. 2023; Li et al. 2024), and (c) a top-heavy initial mass function (IMF) (Inayoshi et al. 2022); although see Cueto et al. (2024). More exotic solutions involving primordial black holes have also been suggested (Liu & Bromm 2022).

³ That is, after reprocessing by the reverse shock that thermalized the ejecta.

2019; Dayal et al. 2022; Priestley et al. 2021). The same argument applies to other known dust sources, such as AGB and evolved stars (Ferrarotti & Gail 2006; Valiante et al. 2009).

As corroborated by the evidence for significant amounts of heavy elements in many super-early galaxies (Curti et al. 2023; Bunker et al. 2023; Calabrò et al. 2024), it is physically sound to assume that dust was also copiously produced by the large number ($\approx 10^7$) of SNe in these galaxies. Moreover, due to the super-early galaxies very compact size, Ferrara (2024a) have shown that in a few million years, the produced dust would completely obscure them. Instead, JWST spectra indicate extremely low V -band attenuations, $A_V \lesssim 0.3$.

To unify several aspects of the problem, it has been proposed that in spite of the high stellar masses, attenuation-free conditions can be established by outflows (Ziparo et al. 2023; Fiore et al. 2023). As the luminosities of super-early objects most often exceed the effective Eddington luminosity for a dusty medium (Ferrara 2024a), which can to first order be translated into a lower bound on the specific star formation rate $sSFR > 25 \text{ Gyr}^{-1}$, they can launch powerful outflows that are driven by radiation pressure on the dust itself.

As $A_V \propto r_d^{-2}$, where r_d is the radial extent of the dust distribution, the outflow can effectively reduce the attenuation by transporting dust on larger spatial scales. For example, an expansion of the distribution from $r_e \approx 200 \text{ pc}$ to $\approx 2 \text{ kpc}$ would cause a dramatic drop in the UV optical depth by 100 times, which would make the galaxy almost transparent and bright. Thus, the AFM predicts that dust is significantly more extended than the stars in super-early galaxies. Moreover, this dust component is thought to emit thermal far-infrared (FIR) continuum by reprocessing the grain of the absorbed UV/optical light from the stars within r_e .

We assess whether the FIR signal produced by this extended dust distribution that is produced by outflows can be detected by the Atacama Large Millimeter Array (ALMA). The detection depends on several factors, such as the (i) spatial extent, (ii) mass, and (iii) temperature (including CMB effects) of the dust, and the (iv) grain optical properties. This experiment represents a stringent test for the AFM.

We mainly concentrate on the specific but yet utmost important case of the most distant known galaxy, GS-z14-0 ($z = 14.32$; Carniani et al. 2024a), for which the required ALMA data will soon become available (DDT 2023.A.00037.S, PI: S. Schouws).

A positive detection would strongly support the idea that dust is produced by SNe and that it is subsequently ejected by outflows outside the galaxy main body. A nondetection would instead place meaningful upper limits on the early dust production and properties at these as yet basically unexplored cosmic epochs. We also applied the model to an additional four $z > 10$ galaxies.

2. FIR dust continuum emission

To predict the expected FIR continuum emission, we first quantified the dust production and its spatial distribution. Next, we computed the dust temperature including the CMB and radiative transfer effects. From these quantities, we finally obtained the observed FIR flux from a given galaxy.

2.1. Dust production

At high redshift ($z > 7$), the dust production can safely be assumed to be largely dominated by SNe (Todini & Ferrara 2001; Leńniewska & Michałowski 2019; Dayal et al. 2022; Sommovigo et al. 2022; Ferrara et al.

2022; Schneider & Maiolino 2024) because grain growth (Ferrara et al. 2016; Hirashita & Aoyama 2019) is subdominant, and the evolution times of other known sources (AGB and evolved stars; Valiante et al. 2009) exceed the Hubble time (294 Myr at $z = 14.32$).

We assumed that stars form according to a Salpeter initial mass function in the range $1\text{--}100 M_\odot$. As a result, an SN occurs every $\nu^{-1} = 52.9 M_\odot$ of stars formed.

The dust yield per SN is rather uncertain because it involves complex nucleation physics of heavy elements in the SN ejecta. Newly formed grains are also subject to destruction processes when they pass through the reverse shock. The net production yield is therefore poorly constrained, but local SN studies (Matsuura et al. 2015; Rho et al. 2018; Priestley et al. 2021; Niculescu-Duvaz et al. 2021) also support that it ranges from 0.01 to $1.1 M_\odot$. Therefore, we used $y_d = 0.1 M_\odot$ as a fiducial value.

Given the IMF, this corresponds to a dust-to-stellar ratio $\xi_d = y_d \nu = 1/529$. However, given the above uncertainties, we explored the implications of the wide range of values $-5 < \log \xi_d < -1.6$. This range should therefore encompass a situation in which freshly formed dust is heavily destroyed by the reverse shock and a super-efficient dust condensation under very favorable conditions.

For the fiducial value of ξ_d and the measured stellar mass of GS-z14-0 ($M_\star = 4 \times 10^8 M_\odot$; Carniani et al. 2024a), we find that $7.5 \times 10^5 M_\odot$ of dust should have been produced by the time of the observation. We recall that dust typically condenses in the ejecta a few hundred days after the explosion (Todini & Ferrara 2001; Nozawa et al. 2007). For our purposes, dust production can be considered as instantaneous and as occurring on the same evolutionary timescale as SN massive star progenitors, that is, $\lesssim 20 \text{ Myr}$.

2.2. Dust spatial distribution

Initially, the dust is distributed as the observed massive stars, providing the observed rest frame UV luminosity. In GS-z14-0, these are distributed within a measured effective radius $r_e = 260 \text{ pc}$. Under this hypothesis, the dust optical depth at 1500 \AA would be equal to $\tau_{1500}^e = (\kappa_{1500} \xi_d / 4\pi r_e^2) M_\star = 23.3$, based on a value of the dust mass absorption coefficient $\kappa_{1500} = 1.26 \times 10^5 \text{ cm}^2 \text{ g}^{-1}$ as appropriate for a MW-like extinction curve (Weingartner & Draine 2001, WD01).

By translating the observed $A_V = 0.31_{-0.07}^{+0.14}$ value into an optical depth using $\tau_{1500} = 2.655(A_V/1.086)$, where the prefactor accounts for the differential attenuation between 1500 \AA and the V band for a MW curve, we find $\tau_{1500} = 0.76$. This value is ≈ 30 times lower than τ_{1500}^e . The value of A_V was inferred from SED modeling (Carniani et al. 2024a), and it might therefore be somewhat degenerate with other fitting quantities. Based on the posterior probability distribution shown in Carniani et al. (2024a) and on the measured blue UV slope ($\beta = -2.2$), we take it that the degeneracy does not represent a serious problem for the model.

Using the AFM to predict the star formation history of GS-z14-0, Ferrara (2024b) found that this galaxy recently underwent a super-Eddington phase in which a powerful outflow mini-quenched its star formation and left it in the observed post-stardust phase. The outflow ejected a significant fraction of the dust, metals, and gas that were previously contained in r_e .

Based on the previous estimates, we see that to decrease A_V to its observed value, the dust has to be reconfigured by the outflow into a much more extended distribution with a radius of $r_d =$

$(\tau_{1500}^e/\tau_{1500})^{1/2}r_e = 5.5r_e$, which corresponds to $r_d \approx 1.4$ kpc for the fiducial ξ_d value.

Without the outflow hypothesis, an extremely low dust content needs to be assumed that corresponds to $\xi_d = 6.6 \times 10^{-5}$ to make the galaxy optically thin. For comparison, for galaxies in the REBELS sample (Bouwens et al. 2022), $\xi_d \approx 0.01$ (Ferrara et al. 2022; Dayal et al. 2022; Sommovigo et al. 2022). The results presented below explore both (and additional) possibilities and show that ALMA observations can clearly distinguish between these two alternative scenarios by detecting the FIR dust emission.

2.3. Dust temperature

Dust grains are heated by absorption of UV photons, whose energy is reemitted in the FIR. Depending on the assumed spatial distribution, the grains can achieve different temperatures, and they thus affect the emitted FIR flux. The latter was computed here at a rest-frame wavelength of $88\mu\text{m}$ since high- z ALMA observations are often tuned to detect [O III] $88\mu\text{m}$ line emission (Popping 2023; Bakx et al. 2022; Kaasinen et al. 2023; Fujimoto et al. 2023b; Kohandel et al. 2023).

The emitted radiation spectrum was classically modeled (e.g. Dayal et al. 2010; Hirashita et al. 2014) as a graybody at a mean dust temperature, \bar{T}_d , given by

$$\bar{T}_d = \left(\frac{L_{\text{abs}}}{\Theta M_d} \right)^{1/(4+\beta_d)}, \quad (1)$$

where

$$\Theta = \frac{8\pi \kappa_{88} k_B^{4+\beta_d}}{c^2 \nu_{88}^{\beta_d} h_P^{3+\beta_d}} \zeta (4 + \beta_d) \Gamma (4 + \beta_d), \quad (2)$$

and $L_{\text{abs}} = L_{\text{bol}}(1 - e^{-\tau_{1500}})$ is the fraction of the stellar UV radiation that is absorbed by dust. The galaxy bolometric luminosity is written as $L_{\text{bol}} = f_{\text{bol}} L_{1500}$, where the intrinsic galaxy luminosity at 1500Å (L_{1500}) was obtained from the inferred star formation rate (SFR) via a conversion factor, $\mathcal{K}_{1500} [L_{\odot}/M_{\odot} \text{yr}^{-1}]$, whose value was chosen so as to match the value used by the ALMA REBELS survey (Bouwens et al. 2022): $\mathcal{K}_{1500} \equiv L_{1500}/\text{SFR} = 0.587 \times 10^{10}$. Following Fiore et al. (2023), we adopted $f_{\text{bol}} = 2$.

We took the mass absorption coefficient κ_{88} and β_d consistently with the adopted WD01 extinction curve $\kappa_{88} = 34.15 \text{cm}^2 \text{g}^{-1}$, and $\beta_d = 2.03$; ζ and Γ are the zeta and gamma functions, respectively. Finally, ν_{88} is the frequency corresponding to a wavelength $\lambda = 88\mu\text{m}$. The other symbols have the usual meaning.

The temperature in Eq. (1) is a mean (or effective) physical dust temperature such that the energy balance between dust absorbed and emitted photon energy is guaranteed. In general, however, radiative transfer effects produce a temperature distribution in which T_d decreases away from the source. It is therefore necessary to include a correction factor, which becomes important when the system becomes optically thick.

Ferrara et al. (2022, see their Appendix A) showed that the luminosity-weighted temperature, $\langle T_d \rangle_L$, of an absorbing dust slab depends on its total optical depth and can be written as

$$\langle T_d \rangle_L = \bar{T}_d \frac{6}{7} \tau_{1500}^{1/b} \frac{(1 - e^{-7\tau_{1500}/b})}{(1 - e^{-\tau_{1500}})^{7/b}} \equiv \bar{T}_d f_L(\tau_{1500}), \quad (3)$$

where $b = 4 + \beta_d$. Applying Eq. (3) results in temperatures that are generally higher⁴ than \bar{T}_d . To conserve energy, M_d must be reduced by a factor $f_L^{-(4+\beta_d)}$. In the following, we denote this reduced dust mass by $M'_d = f_L^{-(4+\beta_d)} M_d$.

2.4. Observed flux at $88\mu\text{m}$

From the previous results, it is straightforward to compute the rest-frame $88\mu\text{m}$ specific flux from a source at $z = z_s$ observed at wavelength $88(1 + z_s)\mu\text{m}$,

$$F_{88} = g(z_s) \kappa_{88} M'_d [B_{88}(T'_d) - B_{88}(T_{\text{CMB}})]. \quad (4)$$

Here, B_{λ} is the blackbody spectrum, and $T_{\text{CMB}}(z) = T_0(1 + z_s)$, with $T_0 = 2.7255 \text{K}$ (Fixsen 2009) is the CMB temperature at redshift z_s . Equation (4) accounts for the fact that the CMB acts as a thermal bath for dust grains and sets a lower limit to their temperature. At $z_s = 14.32$, this minimum temperature corresponds to $T_{\text{CMB}} = 41.75 \text{K}$. Finally, T'_d is the CMB-corrected dust temperature⁵ following Da Cunha et al. (2013),

$$T'_d = \left\{ \langle T_d \rangle_L^{4+\beta_d} + T_0^{4+\beta_d} [(1 + z)^{4+\beta_d} - 1] \right\}^{1/(4+\beta_d)}. \quad (5)$$

3. Results

Figure 1 summarizes our predictions for the ALMA dust continuum emission from GS-z14-0. The top (bottom) panel shows the dependence of the luminosity-weighted dust temperature ($88\mu\text{m}$ flux) for a spherical dust distribution with a varying radius r_d , normalized to the observed effective stellar radius, r_e , of the galaxy. Each curve corresponds to a dust-to-stellar ratio, ξ_d , in the range $-5 < \log \xi_d < -1.6$, equally spaced in 0.1 logarithmic intervals. The black curve highlights the fiducial case $\log \xi_d = -2.72$, or $\xi_d = 1/529$.

The luminosity-weighted temperature trend can be understood with the help of Eq. (3). Along each orange curve, the dust mass $M_d = \xi_d M_{\star}$ is fixed. The most evident feature is the decrease in the dust temperature from $110\text{--}125 \text{K}$ at $r_d = r_e$ to the CMB temperature at the largest considered radii (17.5kpc), where the dust becomes virtually undetectable. The temperature drop arises because at more extended and therefore more optically thin dust distributions, the absorbed stellar radiation decreases and the dust becomes colder. If the dust were not ejected from the galaxy, and therefore $r_d = r_e$, the dust-to-stellar ratio would be very low ($\log \xi_d = -4.2$) to yield the measured $A_V = 0.31$ (denoted by circles).

In addition to this trend, the curves differ by up to $10\text{--}20\%$ at any given radius as a result of variations in M_d from one curve to the next, and because for small radii, most curves (specifically, those with $\log \xi_d > -4.2$) correspond to optically thick regimes for which $\langle T_d \rangle_L$ is slightly higher (see Eq. (3)). This is clearly shown by the optically thick limit $\tau_{1500} \rightarrow \infty$, in which $\langle T_d \rangle_L \propto \tau_{1500}^{1/(4+\beta_d)}$. For each curve, the circles mark the radius at which the attenuation matches the observed value $A_V = 0.31$ (higher/lower A_V values to the left/right). For each value of ξ_d , the temperature indicated by the circle is then the true (i.e., predicted) one within the model assumptions.

⁴ We neglected self-heating by the dust, that is, absorption of thermal IR radiation emitted by the grains, as it becomes important at high optical depth (Gordon et al. 2017), while the configurations of interest here have $A_V < 1$.

⁵ In the remainder of the paper, we refer to the dust temperature as the CMB-corrected one, that is, T'_d in Eq. (5).

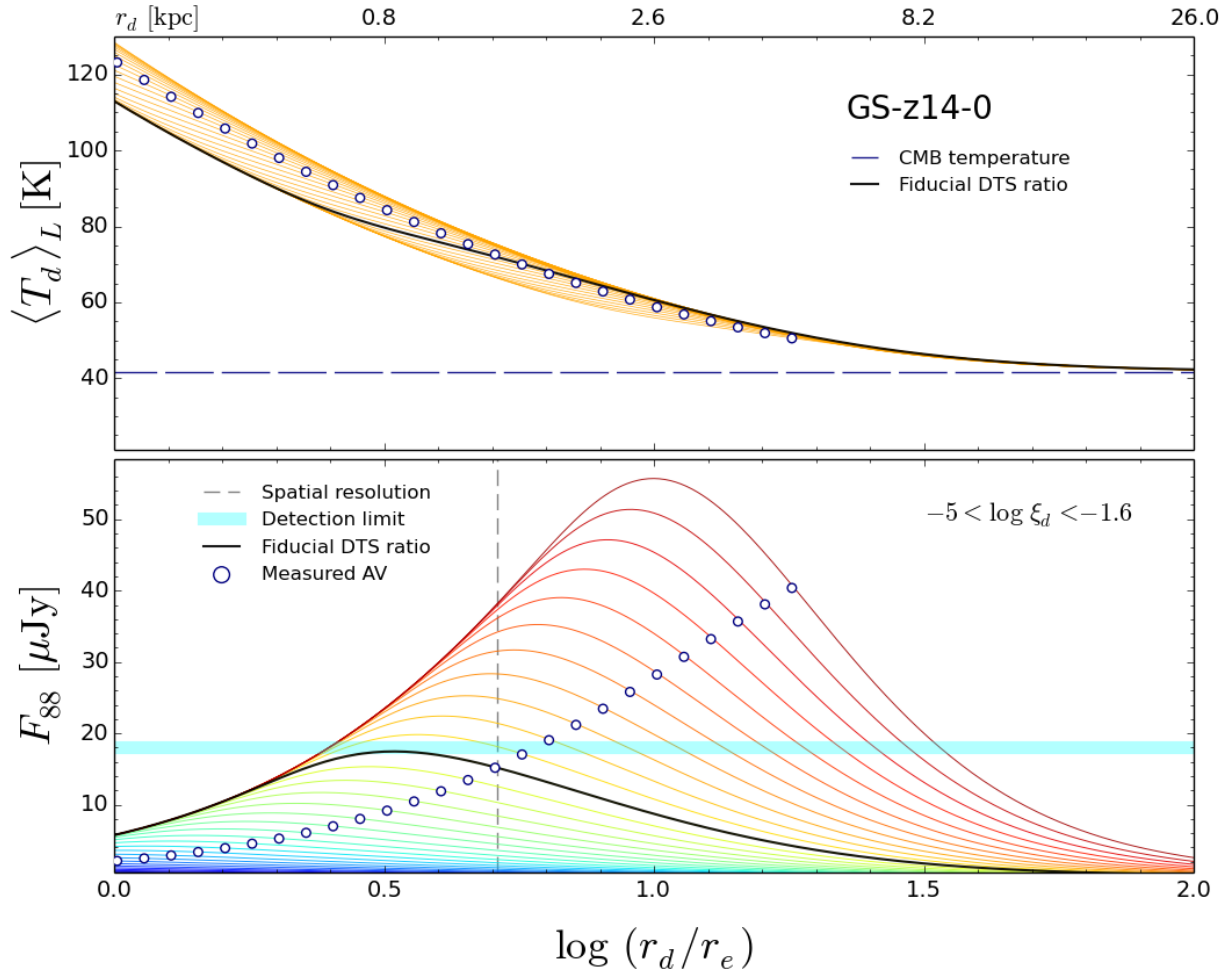


Fig. 1. Model predictions for GS-z14-0. *Top panel:* temperature distribution as a function of the dust spatial distribution radius, r_d , in units of the effective stellar radius of GS-z14-0, $r_e = 260$ pc. The different orange curves span the range of the dust-to-stellar ratio $-5 < \log \xi_d < -1.6$, equally spaced in 0.1 logarithmic intervals. The black curve highlights the fiducial case $\log \xi_d = -2.72$ ($\xi_d = 1/529$). We also show the CMB temperature at the galaxy redshift $z = 14.32$. The circles indicate the radius for which A_V of the galaxy matches the observed radius, $A_V = 0.31$. *Bottom panel:* as in the top panel, but for the predicted observed flux from GS-z14-0 at $88 \mu\text{m}$. We also show the expected 3σ sensitivity limit ($18 \mu\text{Jy}/\text{beam}$) and the spatial resolution ($0.418''$) of the DDT 2023.A.00037.S (PI: S. Schouws) observations.

The behavior of F_{88} in the optically thick regime can be understood as follows. From Eq. (4), further neglecting CMB effects, which is appropriate because dust is hot at small radii, it follows that $F_{88} \propto M' B_\nu(\langle T_d \rangle_L) \approx M' \langle T_d \rangle_L$ in the Rayleigh-Jeans regime. We showed above that $\langle T_d \rangle_L \propto \tau_{1500}^{1/(4+\beta_d)}$; also, $M'_d = f_L^{-(4+\beta_d)} M_d \propto \tau_{1500}^{-1}$. Hence, F_{88} decreases as $\tau_{1500}^{-(3+\beta_d)/(4+\beta_d)}$, which is exactly the trend shown in Fig. 1.

The corresponding $88 \mu\text{m}$ flux is shown in the bottom panel, where it is also compared with the expected 3σ continuum sensitivity ($18 \mu\text{Jy}/\text{beam}$) and the spatial resolution ($0.451''$) of the ALMA DDT 2023.A.00037.S (PI: S. Schouws) observations of GS-z14-0. For each ξ_d value, the flux rises, reaches a peak (approximately where $\tau_{1500} \approx 1$), and decreases at large radii. The amplitude of the peak correlates with ξ_d . As the distribution becomes optically thick for low r_d/r_e values, the curves with larger ξ_d (or, equivalently, higher M_d) converge to a single line.

The circles ($A_V = 0.31$) show that the fiducial model (black line, $\xi_d = 1/529$) predicts a $88 \mu\text{m}$ flux $F_{88}^{\text{fid}} = 14.9 \mu\text{Jy}$, essentially at the 3σ detection limit of the experiment, and a luminosity-weighted temperature of 72 K . As ξ_d decreases, implying an efficient grain destruction by interstellar shocks, the signal becomes weaker and more difficult to detect. How-

ever, if the galaxy is dust rich, at or above the level observed in some of the REBELS galaxies showing $\xi_d \approx 0.01$ (Ferrara et al. 2022; Dayal et al. 2022; Inami et al. 2022), the signal becomes detectable.

It is important to recall that the observed F_{88} measurement (or upper limit) should be interpreted along with the constraints provided by the observed A_V value. For example, we assumed that consistently with the fiducial model in Fig. 2, F_{88} is measured to be $14.9 \mu\text{Jy}$ (circle on the black curve). We then conclude that $\xi_d = 1/529$, and $\log(r_d^{\text{fid}}/r_e) \approx 0.7$, or $r_d = 1.3 \text{ kpc}$. If this were correct, ALMA observations should also show that the dust is spatially resolved and more extended than the stellar component. The other more compact solution for the same F_{88} , that is, $\log(r_d/r_e) \approx 0.4$, should be discarded because the galaxy would have an A_V much higher than observed.

The natural case to explore is the case in which the dust in the absence of any ejective event remains within r_e . In this scenario, the temperature would be significantly higher ($\approx 100 \text{ K}$) and the distribution would be optically thick. These two properties act to dramatically suppress the flux: Regardless of ξ_d (unless it is extremely small), $F_{88} = 5.3 \mu\text{Jy}$. Detecting such a low flux would require very long integration times.

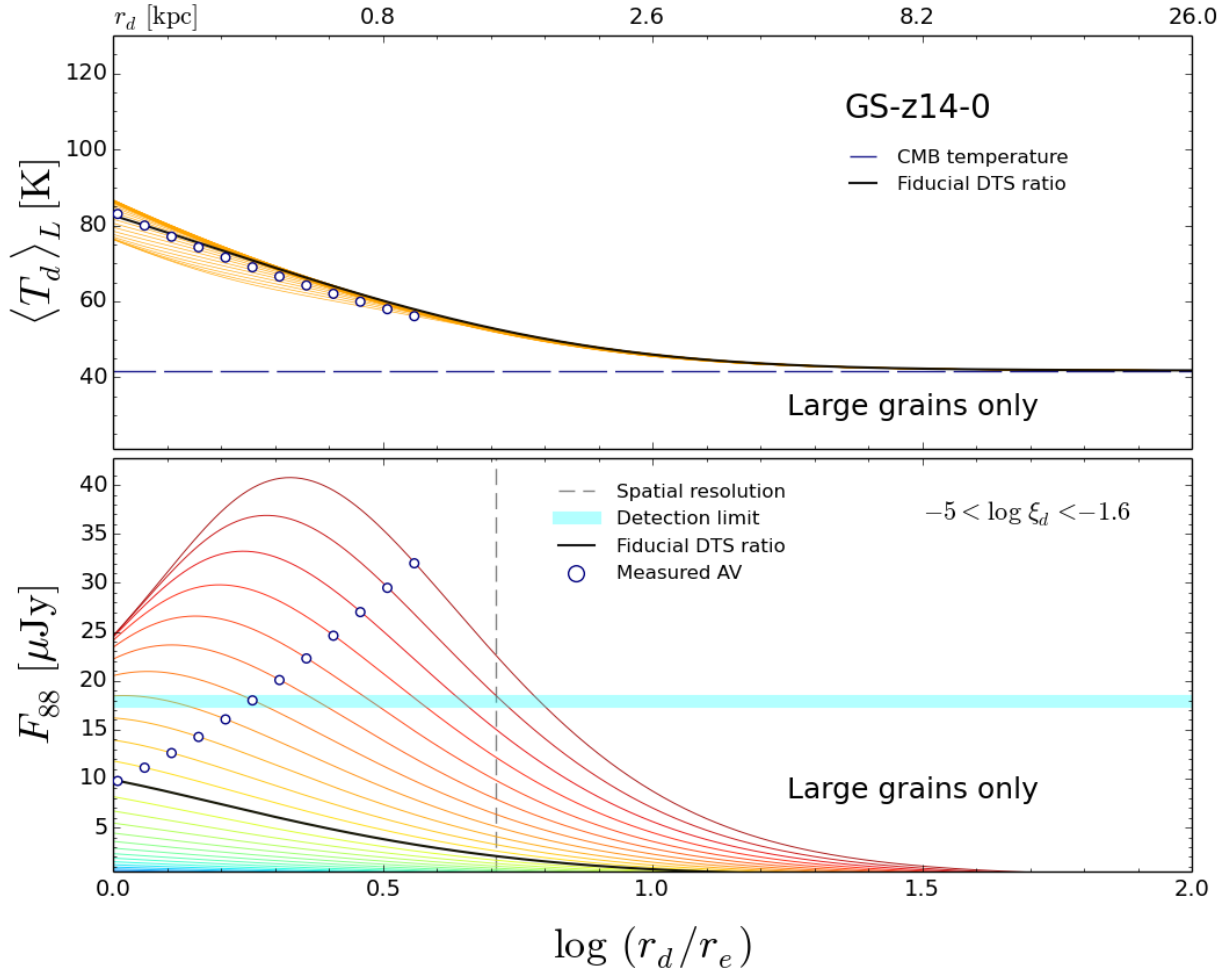


Fig. 2. Same as Fig. 1, but assuming that the dust consists of large silicate grains with a log-normal distribution centered at $0.5 \mu\text{m}$, as appropriate for grains that freshly formed in SN ejecta.

In conclusion, a positive detection would strongly support the hypothesis that dust produced by SNe associated with the observed stars in GS-z14-0 has been carried to larger galactocentric radii by outflows. This causes the galaxy to become bright and transparent to UV radiation. This conclusion highlights the key importance of ALMA deep observations of super-early galaxies.

3.1. Large grains

In addition to dust ejection or destruction by shocks, we considered a third possibility, that is, that early dust consists of large grains with sizes of $0.1\text{--}1 \mu\text{m}$. This is based on two facts: (a) It is theoretically predicted that SN dust lacks small grains, which are preferentially destroyed in the ejecta by the reverse shock (Nozawa et al. 2007; Asano et al. 2013; Hirashita & Aoyama 2019). (b) Experimentally, the SED of galaxies in $z = 2\text{--}12$ JWST-detected galaxies shows an increasingly flatter extinction curve toward high- z (Di Mascia et al. 2021; Markov et al. 2024). These two pieces of evidence are clearly connected because large grains of size a absorb light with a wavelength $\lambda \ll a$ in a frequency-independent way. In this case, the absorption cross section should be equal to the geometric one, and the UV absorption coefficient $\kappa_{\text{UV}}^{\text{large}} \approx 3/4\delta_g a$, where $\delta_g = 2.95 \text{ g cm}^{-3}$ is the material density of silicate grains, that is,

those that are preferentially produced by SNe. If $a = 0.5 \mu\text{m}$, $\kappa_{\text{UV}}^{\text{large}} = 0.04\kappa_{\text{UV}}$.

These estimates were confirmed by detailed calculations performed by Ysard et al. (2019), which we used here. These authors computed the optical properties of $0.01 \mu\text{m}$ to 10 cm grains from effective medium and Mie theories. To do this, they assumed a log-normal distribution of the grain sizes centered at a given radius, a_0 , which we assumed to be equal to $0.5 \mu\text{m}$ according to the previous discussion, and a fixed dispersion $\sigma = 0.7$. With these assumptions, they indeed found $\kappa_{\text{UV}}^{\text{large}} \approx 3/4\delta_g a = 5085 \text{ cm}^2 \text{ g}^{-1}$ and $\kappa_{88}^{\text{large}} = 15 \text{ cm}^2 \text{ g}^{-1}$.

Figure 2 presents the temperature and expected flux if dust is composed of large $\approx 0.5 \mu\text{m}$ grains. The temperature follows the same trend as in the standard case, but it is significantly colder. It reaches values in the range $75\text{--}85 \text{ K}$ at r_e . As a result, for any given ξ_d , the flux is lower, for instance, $F_{88}^{\text{fid}} = 9.5 \mu\text{Jy}$, and it shifts to smaller radii compared to the standard case. The lower opacity of large grains also allows the galaxy to become optically thin (as observed) for more compact distributions.

3.2. Other super-early galaxies

Our model can be used to predict the FIR observability of other potentially detectable super-early galaxies. In addition to GS-z14-0, which has the largest A_V of the $z > 10$ spectroscopically

Table 1. Relevant properties of the selected super-early galaxies at $z > 10$.

ID	redshift	A_V [mag]	SFR [$M_\odot \text{yr}^{-1}$]	$\log(M_\star/M_\odot)$	r_e [pc]	F_{88}^{fid} [μJy]	F_{88}^{max} [μJy]	$\log(r_d^{\text{fid}}/r_e)$
GS-z14-0 ^(a)	14.32	$0.31^{+0.14}_{-0.07}$	22^{+6}_{-6}	$8.60^{+0.7}_{-0.2}$	260^{+2}_{-2}	14.9	40.1	0.73
GS-z14-1 ^(a)	13.90	$0.20^{+0.11}_{-0.07}$	$2^{+0.7}_{-0.4}$	$8.00^{+0.4}_{-0.4}$	< 160	2.0	3.8	0.70
UNCOVER-z12 ^(b)	12.39	$0.19^{+0.17}_{-0.10}$	$3.08^{+1.81}_{-0.68}$	$8.35^{+0.21}_{-0.16}$	426^{+40}_{-42}	4.4	8.5	0.47
GS-z11-0 ^(c)	11.58	$0.18^{+0.06}_{-0.06}$	$2.20^{+0.28}_{-0.22}$	$8.67^{+0.08}_{-0.13}$	77 ^(†)	5.2	7.8	1.38
GHZ2 ^(d)	12.34	$0.04^{+0.07}_{-0.03}$	$5.2^{+1.1}_{-0.6}$	$9.05^{+0.10}_{-0.25}$	105^{+9}_{-9}	3.4	4.0	1.76

Notes. The measured values are taken from the following references: ^(a)Carniani et al. (2024a), Robertson et al. (2024); ^(b)Wang et al. (2023), Fujimoto et al. (2023a), Atek et al. (2023); ^(c)Curtis-Lake et al. (2023), Robertson et al. (2024); ^(d)Castellano et al. (2024); ^(†)Error not provided. The last three columns show the predictions of the model for the fiducial (maximum) 88 μm observed flux, and the fiducial dust-to-stellar radius ratio for which A_V matches the observed value, respectively.

confirmed galaxies, we selected the next three dustiest galaxies, GS-z14-1 ($A_V = 0.20$), UNCOVER-z12 (0.19), and GS-z11-0 (0.18). We also included GHZ2 in spite of its very low attenuation ($A_V = 0.04$; Castellano et al. 2024, but see Zavala et al. 2025, who found $A_V = 0.01\text{--}0.2$ depending on the SED fitter used) because of its spectrum is very interesting and shows many prominent emission lines.

The relevant properties (redshift, A_V , SFR, M_\star , and r_e) of the galaxies in the sample are reported in Table 1, along with the predicted value of the fiducial 88 μm flux and the radius r_d^{fid} at which the attenuation becomes equal to the observed A_V value. We also show the maximum expected flux, F_{88}^{max} , which we took from the curve with the maximum assumed value of $\log \xi_d = -1.6$.

For the galaxies in the sample, the dust temperature and FIR flux follow very similar trends with r_d/r_e , as shown in Fig. 1 for GS-z14-0, but they differ quantitatively as a result of the different properties of the galaxy. The table shows that the expected fiducial fluxes range from 2 μJy for the faintest galaxy (GS-z14-1) to 14.9 μJy for the brightest (and most distant) galaxy, GS-z14-0. The latter therefore remains the most promising target for constraining the dust content of the very early galaxies. When we instead assume the largest attenuation found by Zavala et al. (2025), $A_V = 0.2$, we find a larger fiducial and maximum flux for GHZ2, $F_{88}^{\text{fid}} = 11.2 \mu\text{Jy}$ and $F_{88}^{\text{max}} = 16.3 \mu\text{Jy}$, respectively.

Finally, we did not consider the remarkable galaxy GN-z11 (Bunker et al. 2023) because it is not visible by ALMA: It is located in the northern hemisphere location. However, this galaxy has been observed by the Northern Extended Millimeter Array (NOEMA; Fudamoto et al. 2024). These observations placed a 1σ upper limit of 13 $\mu\text{Jy}/\text{beam}$ at 160 μm . When this was applied to GN-z11, our model (fiducial case) predicted a maximum flux $F_{160}^{\text{max}} = 14.1 \mu\text{Jy}$. Although interesting, available NOEMA observations are unfortunately too shallow for detecting the expected signal.

4. Summary

To test one of the predictions of the AFM (Ferrara et al. 2023; Ferrara 2024a), we modeled the FIR dust continuum emission from the extended dust distribution produced by outflows around so-called blue monsters, that is, luminous blue super-early ($z > 10$) galaxies. Based on the observed properties of the galaxies (redshift, A_V , SFR, M_\star , and r_e), the expected flux at 88 μm depends on the dust-to-stellar ratio, ξ_d , and on the extent of the dust distribution, r_d . A signal detection with ALMA would there-

fore constrain the amount of dust and its extent, thus representing a successful test that the attenuation-free conditions are produced by dust ejection by (likely, radiation-driven) outflows. We discussed in detail GS-z14-0 ($z = 14.32$), and we further applied the model to another four super-early galaxies. Our results are listed below.

- When the dust is in the galaxy ($r_d = r_e$), its temperature is 110–125 K. In this case, the dust-to stellar mass ratio must be very low ($\log \xi_d < -4.2$), however, so that it does not exceed the measured $A_V = 0.31$. For $r_d > r_e$, $\langle T_d \rangle_L$ decreases asymptotically toward T_{CMB} (Fig. 1, top panel).
- The fiducial model ($\xi_d = 1/529$) predicts an observed flux $F_{88}^{\text{fid}} = 14.9 \mu\text{Jy}$ for GS-z14-0 and a dust extent $r_d \sim 1.4 \text{ kpc}$ (Fig. 1, bottom panel). For the highest value we considered, $\log \xi_d = -1.6$, $F_{88}^{\text{max}} = 40.1 \mu\text{Jy}$. These values are lower ($F_{88}^{\text{fid}} = 9.5 \mu\text{Jy}$) when the dust predominantly consists of large grains, such as those that form in SN ejecta (Fig. 2).
- Forthcoming ALMA observations, with an expected 3σ sensitivity of 18 μJy , should come very close to constraining the fiducial predictions of the outflow-based attenuation-free model.
- Other super-early galaxies are predicted (Table 1) to be fainter at 88 μm , mostly because their SFR is lower than that of GS-z14-0, but also because their A_V is lower, with fiducial fluxes in the range $F_{88}^{\text{fid}} = 2\text{--}5.2 \mu\text{Jy}$.

We conclude by cautioning that although our model was built to catch the main features of the AFM, its simple incarnation cannot include potentially non-negligible effects that might change our conclusions quantitatively. For example, our study does not account for self-heating of the dust by reprocessed thermal photons, dust scattering, and grain size distribution. The impact of these effects on the results presented here can only be ascertained via dedicated numerical radiative transfer simulations.

After submission of this manuscript, two different groups (Schouws et al. 2024; Carniani et al. 2024b) have presented the analysis of the ALMA DDT observations of GS-z14-0. Both groups reported no dust continuum detection at 88 μm (upper limits $F_{88\mu\text{m}} < 15.1 \mu\text{Jy}$). This suggests an upper limit on the dust-to-stellar mass ratio of $< 2 \times 10^{-3}$ according to the AFM, which is consistent with dust production from supernovae with a yield $y_d < 0.3 M_\odot$. We refer to these papers for a more extended discussion.

Acknowledgements. We thank J. Zavala and M. Castellano for useful discussions, data and comments. This work is supported by the ERC Advanced Grant INTERSTELLAR H2020/740120, and in part by grant NSF PHY-2309135 to

the Kavli Institute for Theoretical Physics (KITP). Plots in this paper produced with the MATPLOTLIB (Hunter 2007) package for PYTHON.

References

- Arrabal Haro, P., Dickinson, M., Finkelstein, S. L., et al. 2023a, *Nature*, **622**, 707
- Arrabal Haro, P., Dickinson, M., Finkelstein, S. L., et al. 2023b, *ApJ*, **951**, L22
- Asano, R. S., Takeuchi, T. T., Hirashita, H., & Inoue, A. K. 2013, *Earth Planets Space*, **65**, 213
- Atek, H., Shuntov, M., Furtak, L. J., et al. 2023, *MNRAS*, **519**, 1201
- Bakx, T. J. L. C., Zavala, J. A., Mitsuhashi, I., et al. 2022, *MNRAS*, **519**, 5076
- Bouwens, R. J., Smit, R., Schouws, S., et al. 2022, *ApJ*, **931**, 160
- Bunker, A. J., Saxena, A., Cameron, A. J., et al. 2023, *A&A*, **677**, A88
- Calabrò, A., Castellano, M., Zavala, J. A., et al. 2024, *ApJ*, **975**, 245
- Carniani, S., Hainline, K., D'Eugenio, F., et al. 2024a, *Nature*, **633**, 318
- Carniani, S., D'Eugenio, F., Ji, X., et al. 2024b, *A&A*, submitted [arXiv:2409.20533]
- Castellano, M., Napolitano, L., Fontana, A., et al. 2024, *ApJ*, **972**, 143
- Cueto, E. R., Hutter, A., Dayal, P., et al. 2024, *A&A*, **686**, A138
- Curti, M., D'Eugenio, F., Carniani, S., et al. 2023, *MNRAS*, **518**, 425
- Curtis-Lake, E., Carniani, S., Cameron, A., et al. 2023, *Nat. Astron.*, **78**, 622
- Da Cunha, E., Groves, B., Walter, F., et al. 2013, *ApJ*, **766**, 13
- Dayal, P., Hirashita, H., & Ferrara, A. 2010, *MNRAS*, **403**, 620
- Dayal, P., Ferrara, A., Sommovigo, L., et al. 2022, *MNRAS*, **512**, 989
- Dekel, A., Sarkar, K. C., Birnboim, Y., Mandelker, N., & Li, Z. 2023, *MNRAS*, **523**, 3201
- Di Mascia, F., Gallerani, S., Behrens, C., et al. 2021, *MNRAS*, **503**, 2349
- Ferrara, A. 2024a, *A&A*, **684**, A207
- Ferrara, A. 2024b, *A&A*, **689**, A310
- Ferrara, A., Viti, S., & Ceccarelli, C. 2016, *MNRAS*, **463**, L112
- Ferrara, A., Sommovigo, L., Dayal, P., et al. 2022, *MNRAS*, **512**, 58
- Ferrara, A., Pallottini, A., & Dayal, P. 2023, *MNRAS*, **522**, 3986
- Ferrarotti, A. S., & Gail, H. P. 2006, *A&A*, **447**, 553
- Finkelstein, S. L., Leung, G. C. K., Bagley, M. B., et al. 2023, ArXiv e-prints [arXiv:2311.04279]
- Fiore, F., Ferrara, A., Bischetti, M., Feruglio, C., & Travascio, A. 2023, *ApJ*, **943**, L27
- Fixsen, D. J. 2009, *ApJ*, **707**, 916
- Fudamoto, Y., Oesch, P. A., Walter, F., et al. 2024, *MNRAS*, **530**, 340
- Fujimoto, S., Wang, B., Weaver, J., et al. 2023a, ArXiv e-prints [arXiv:2308.11609]
- Fujimoto, S., Finkelstein, S. L., Burgarella, D., et al. 2023b, *ApJ*, **955**, 130
- Gordon, K. D., Baes, M., Bianchi, S., et al. 2017, *A&A*, **603**, A114
- Helton, J. M., Rieke, G. H., Alberts, S., et al. 2024, ArXiv e-prints [arXiv:2405.18462]
- Hirashita, H., & Aoyama, S. 2019, *MNRAS*, **482**, 2555
- Hirashita, H., Ferrara, A., Dayal, P., & Ouchi, M. 2014, *MNRAS*, **443**, 1704
- Hsiao, T. Y.-Y., Coe, D., Larson, R. L., et al. 2024, *ApJ*, **973**, 8
- Hunter, J. D. 2007, *Comput. Sci. Eng.*, **9**, 90
- Inami, H., Algera, H. S. B., Schouws, S., et al. 2022, *MNRAS*, **515**, 3126
- Inayoshi, K., Harikane, Y., Inoue, A. K., Li, W., & Ho, L. C. 2022, *ApJ*, **938**, L10
- Kaasinen, M., van Marrewijk, J., Popping, G., et al. 2023, *A&A*, **671**, A29
- Kohandel, M., Ferrara, A., Pallottini, A., et al. 2023, *MNRAS*, **520**, L16
- Leńniewska, A., & Michałowski, M. J. 2019, *A&A*, **624**, L13
- Li, Z., Dekel, A., Sarkar, K. C., et al. 2024, *A&A*, **690**, A108
- Liu, B., & Bromm, V. 2022, *ApJ*, **937**, L30
- Markov, V., Gallerani, S., Ferrara, A., et al. 2024, ArXiv e-prints [arXiv:2402.05996]
- Martínez-González, S., Wunsch, R., Silich, S., et al. 2019, *ApJ*, **887**, 198
- Mason, C. A., Trenti, M., & Treu, T. 2023, *MNRAS*, **521**, 497
- Matsuura, M., Dwek, E., Barlow, M. J., et al. 2015, *ApJ*, **800**, 50
- Mirocha, J., & Furlanetto, S. R. 2023, *MNRAS*, **519**, 843
- Naidu, R. P., Oesch, P. A., van Dokkum, P., et al. 2022, *ApJ*, **940**, L14
- Niculescu-Duvaz, M., Barlow, M. J., Bevan, A., Milisavljevic, D., & De Looze, I. 2021, *MNRAS*, **504**, 2133
- Nozawa, T., Kozasa, T., Habe, A., et al. 2007, *ApJ*, **666**, 955
- Nozawa, T., Kozasa, T., Tominaga, N., et al. 2010, *ApJ*, **713**, 356
- Pallottini, A., & Ferrara, A. 2023, *A&A*, **677**, L4
- Planck Collaboration XVI. 2014, *A&A*, **571**, A16
- Popping, G. 2023, *A&A*, **669**, L8
- Priestley, F. D., De Looze, I., & Barlow, M. J. 2021, *MNRAS*, **502**, 2438
- Rho, J., Gomez, H. L., Boogert, A., et al. 2018, *MNRAS*, **479**, 5101
- Robertson, B., Johnson, B. D., Tacchella, S., et al. 2024, *ApJ*, **970**, 31
- Schneider, R., & Maiolino, R. 2024, *A&ARv*, **32**, 2
- Schouws, S., Bouwens, R. J., Ormerod, K., et al. 2024, ArXiv e-prints [arXiv:2409.20549]
- Sommovigo, L., Ferrara, A., Pallottini, A., et al. 2022, *MNRAS*, **513**, 3122
- Tacchella, S., Eisenstein, D. J., Hainline, K., et al. 2023, *ApJ*, **952**, 74
- Todini, P., & Ferrara, A. 2001, *MNRAS*, **325**, 726
- Valiante, R., Schneider, R., Bianchi, S., & Andersen, A. C. 2009, *MNRAS*, **397**, 1661
- Wang, B., Fujimoto, S., Labbé, I., et al. 2023, *ApJ*, **957**, L34
- Weingartner, J. C., & Draine, B. T. 2001, *ApJ*, **548**, 296
- Ysard, N., Koehler, M., Jimenez-Serra, I., Jones, A. P., & Verstraete, L. 2019, *A&A*, **631**, A88
- Zavala, J. A., Castellano, M., Akins, H. B., et al. 2025, *Nat. Astron.*, **9**, 155
- Ziparo, F., Ferrara, A., Sommovigo, L., & Kohandel, M. 2023, *MNRAS*, **520**, 2445